Analysis of Transport in a CVD Silicon Carbide Deposition Reactor

MARIA A. KUCZMARSKI
NASA Lewis Research Center
Cleveland, OH 44135

ABSTRACT: A reactor for chemical vapor deposition of silicon carbide from silane and propane in hydrogen was modeled using the commercial software package FLUENT. A chemical reaction mechanism including both homogeneous and heterogeneous reactions was incorporated into the model. Two different pressures were modeled: 2.7 kPa and 101 kPa. Streaklines were used to visualize the flow inside the reactor. The flux of silicon and carbon to the growth surface was also examined. Dimensionless numbers were utilized to provide insights into the relative magnitudes of convection and diffusion in the reactor. The modeling results indicated that silicon carbide deposition is limited by both the depletion of carbon and by the limited reactivity of propane. Non-uniform deposition results from both non-uniform flow patterns in the reactor and large concentration gradients arising from diffusional limitations.

KEY WORDS: modeling, CVD, silicon carbide.

1. INTRODUCTION

Chemical vapor deposition (CVD) is used extensively for depositing solid films from gaseous precursors onto a solid substrate. In the microelectronics industry, CVD is an important method for depositing semiconductor materials of exceptionally high purity. As the requirements for materials produced by CVD become more stringent, it becomes essential to develop a method of analyzing such systems. Mathematical models can be used to relate reactor performance variables to operating conditions, and to aid in the design of new reactors.

The commercially available code FLUENT [1] can model not only the

Reprinted from *Journal of* CHEMICAL VAPOR DEPOSITION, Vol. 2—*July 1993*

fluid flow and heat transfer within the reactor, but the multiple chemical reactions which occur during CVD as well [2–4]. This code was utilized to study the transport inside a reactor for the deposition of silicon carbide for semiconductor applications.

2. MODEL

The model was based on the silicon carbide deposition reactor in use in the High Temperature Integrated Electronics and Sensors Program at the NASA Lewis Research Center. This reactor consists of a horizontal, water-cooled quartz tube (0.0508 m in diameter, 0.515 m in length) and a silicon carbide-coated graphite susceptor, held by a quartz support, on which the growth substrate is placed. Radio frequency (RF) coils around the quartz tube inductively heat the susceptor, which heats the substrate. Modeling runs were conducted for both 2.7 kPa and 101 kPa, although experimental data is currently available only at 101 kPa.

The version of FLUENT available during the course of this work was unable to model the exact geometry of the silicon carbide reactor. As an approximation, a square cross-section was assumed and the inlet flow rate in the model was adjusted to maintain the same mass flow rate as in the experimental reactor. This reactor, shown in Figure 1, was used

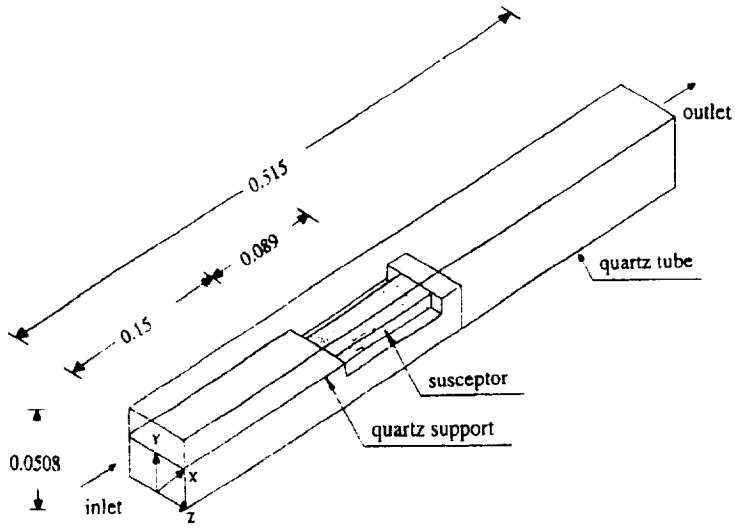

Figure 1. Reactor for silicon carbide growth used in model. All dimensions are in meters.

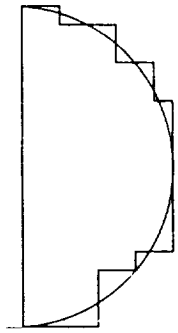

Figure 2. Approximation to a circular cross-section used in model.

to examine the flow patterns in the reactor. An approximation to a circular cross-section, shown in Figure 2, was later made and used to obtain the results presented in the rest of the paper. Half of a circular cross-section is shown, along with approximating steps used to define the model boundaries.

The plane of symmetry along the axis of the reaction tube (plane at Z = 0) allowed half of the reactor to be modeled in order to decrease computation time. The computational grid contained 36 cells in the X-direction, 16 cells in the Y-direction, and 12 cells in the Z-direction. A non-uniform grid was utilized to compress the size of the cells in areas where high gradients were expected, such as near the growth surface. The reactor inlet and exit were shortened by five centimeters each in the model without a change in the flow and temperature fields over the growth surface, allowing a greater concentration of cells throughout the rest of the reactor.

The governing equations used in this model are given below:

conservation of mass:

$$\frac{\partial}{\partial x_i}(\varrho u_i) = 0 \tag{1}$$

conservation of momentum:

$$\frac{\partial}{\partial x_i}(\varrho u_i u_j) = \frac{\partial}{\partial x_i}\left(\mu\left[\frac{\partial u_i}{\partial x_j} + \frac{\partial u_j}{\partial x_i}\right]\right) - \frac{\partial P}{\partial x_i} + \varrho g_i \tag{2}$$

conservation of energy:

$$\frac{\partial}{\partial x_i}(\varrho u_i h) = \frac{\partial}{\partial x_i}\left(k\frac{\partial T}{\partial x_i}\right) \tag{3}$$

conservation of chemical species:

$$\frac{\partial}{\partial x_i}(\varrho u_i X_i) = \frac{\partial J_i}{\partial x_i} + R_i \tag{4}$$

where:

u_i = velocity in the ith direction (m/s)
x_i = distance in the ith direction (m)
ϱ = density (kg/m^3)
μ = Newtonian viscosity (kg/m s)
P = pressure (Pa)
g = gravity (m/s^2)
h = enthalpy (J/kg)
k = thermal conductivity (W/m K)
T = temperature (K)
X_i = mass fraction of species i (dimensionless)
J_i = flux of species i (kg/m^{2}s)
R_i = mass rate of creation or depletion of species i by chemical reaction (kg/m^{3}s)

Density was computed from the ideal gas law:

$$\varrho = \frac{P}{RT\sum_i \frac{X_i}{M_i}} \tag{5}$$

where:

R = universal gas constant (J/kgmoles K)
M_i = molecular weight (kg/kgmoles)

The diffusional flux of species i, J_i, that arises from concentration gradients and thermal gradients (the Soret effect), is given by:

$$J_i = -\varrho D_i\left(\frac{\partial X_i}{\partial x_i}\right) - \left[\frac{D_i^T}{T}\left(\frac{\partial T}{\partial x_i}\right)\right] \tag{6}$$

where:

D_i^T = thermal diffusion coefficient (kg/m²)
D_{im} = diffusion coefficient of species i in the mixture (kg/m²)

This expression is only valid when the diffusion coefficient is independent of composition. This was assumed to be valid in this case because of the dilute concentration of the source gases in the hydrogen carrier gas.

Reactions occur in the gas phase or at a surface. The rate expression is:

$$R_{ik} = V_{ik} M_i T^{(\beta_k)} A_k \prod_{j \text{ reactants}} [C_j]^{(\nu_{jk})} \exp\left(\frac{-(E_a)_k}{RT}\right) \tag{7}$$

where:

R_{ik} = rate of creation or destruction of species i in reaction k (kg/m³s)
V_{ik} = molar stoichiometry coefficient for species i in reaction k (dimensionless)
M_i = molecular weight of species i (kg/kgmoles)
T = temperature (K)
β_k = temperature exponent for Arrhenius rate (dimensionless)
A_k = preexponential factor for Arrhenius rate (time^{-1}/concentration^{n-1}), n is the reaction order
$[C_j]$ = molar concentration of each reactant species j (kgmoles/m³)
ν_{jk} = exponent on concentration of reactant j in reaction k (dimensionless)
E_k = activation energy (J/kgmole)
R = universal gas constant (J/kgmole K)

The inlet velocity was 0.025 m/s at 101 kPa and 0.95 m/s at 2.7 kPa. The molar flow rate was held fixed as the pressure was lowered. A velocity of zero was specified at the surface of the susceptor, the quartz support and the reactor walls. Constant temperatures of 280 K at the inlet and reactor walls, and 1723 K at the susceptor were specified. The temperature distribution in the quartz support was calculated from the conduction equation:

$$\nabla \cdot k_w \nabla T = 0 \tag{8}$$

where k_w is the thermal conductivity of quartz. Inlet mole fractions were 0.00028 for silane and 0.00011 for propane. At the surface of the susceptor and the quartz support, the mass diffusion of a species to the surface was balanced by its rate of creation or destruction by surface reactions:

$$-\varrho D_i \left(\frac{\partial X_i}{\partial \hat{n}}\right) = \sum_{k=1} R_{ik} \tag{9}$$

where n is the unit vector normal to the surface, and the summation includes surface reactions. Since the walls of the reactor were at such a low temperature, it was assumed the reactions would not be occurring to a significant extent at the reactor walls; a zero total flux condition was used for all species at the boundary instead. Radiation heat transfer was not included in this model, since the reactor wall was kept at a uniform temperature.

Since each species and reaction in the model greatly increased the required computation time, it was necessary to devise the smallest chemistry set which still accurately described the deposition process. To further decrease computation time, two cases were run for each set of reactor conditions: one containing reactions involving only silicon-containing species and one containing reactions involving only carbon-containing species. This approach should be valid if there are no significant concentrations of growth species containing both silicon and carbon, which previous modeling work has indicated is the case [5–7]. The chemistry sets for both silicon and carbon deposition were chosen based on a review of the literature, while working within the constraints imposed by FLUENT.

The chemical reactions used to describe silicon deposition are shown in Table 1; the reaction rate data are given in Appendix A. The key silicon-containing species contributing to silicon carbide growth from

Table 1. Silicon chemistry set for silicon carbide growth.

Reaction	Type	
$SiH_4 \rightarrow SiH_2 + H_2$	gas phase	(S1)
$SiH_2 + H_2 \rightarrow SiH_4$	gas phase	(S2)
$Si_2H_6 \rightarrow SiH_4 + SiH_2$	gas phase	(S3)
$SiH_4 + SiH_2 \rightarrow Si_2H_6$	gas phase	(S4)
$SiH_4 \rightarrow Si + 2H_2$	surface	(S5)
$SiH_2 \rightarrow Si + H_2$	surface	(S6)
$Si_2H_6 \rightarrow 2Si + 3H_2$	surface	(S7)

silane and propane appear to be SiH_4 and SiH_2 [7]. However, SiH_2 can rapidly insert itself into silane to form Si_2H_6 [8]; therefore, inclusion of Si_2H_6 provides a more complete model. Inclusion of higher silanes could be important in non-hydrogen carrier gases; however, their concentrations are suppressed in a hydrogen carrier gas, implying that they do not constitute a major pathway for decomposition [8]. SiH_3 is not believed to be important to the initial dissociation mechanism because of the high bond dissociation energy for removing a hydrogen from SiH_4; therefore, this species is not included in the model [8]. Gas phase reaction rates in Appendix A were taken from [8]; surface reaction rates were determined using sticking coefficients and collision rates from kinetic theory:

$$R_i^{surface} = \left[\frac{RT}{2\pi M_i}\right]^{0.5} S_i \varrho X_i \tag{10}$$

where S_i is the sticking coefficient, the ratio of the number of molecules of species i that react when striking the surface to the total number of molecules of species i striking the surface. Since the concentration of a species will decrease with pressure according to the ideal gas law, the rates of the surface reactions, dependent on the species concentrations, will also decrease.

The chemical reactions used to describe carbon deposition are given in Table 2; reaction rate data is given in Appendix B. Previous modeling of silicon carbide deposition from silane and propane has indicated that C_2H, C, and species involving four or more carbon atoms are present in very small concentrations at high temperatures, and, therefore, do not significantly contribute to the deposition rate [9]. The major contributing species appear to be C_3H_8, C_2H_4, C_2H_2, CH_4, and CH_3, with the relative importance of each depending upon the substrate temperature [7]. Gas phase reaction rates in Appendix B were taken from [10]. Rate constants determined under conditions matching as closely as possible those of the actual reactor were chosen. Surface reaction rates were determined using sticking coefficients and collision rates from kinetic theory, as described by Equation (10). The rates of surface reactions, as described previously, will decrease with decreasing pressure.

Silicon-carbon bonds most probably form on the deposition surface to produce silicon carbide; however, information on the rate constants for such reactions is presently unavailable. Therefore, the growth rate of silicon carbide must be obtained from the individual deposition rates of silicon and carbon. Since stoichiometric deposits of silicon carbide are obtained in practice [11], an approximate growth rate can be obtained

Table 2. Carbon chemistry set for silicon carbide growth.

Reaction	Type	
$C_3H_8 \rightarrow CH_3 + C_2H_5$	gas phase	(C1)
$CH_3 + C_2H_5 \rightarrow C_3H_8$	gas phase	(C2)
$CH_3 + H_2 \rightarrow CH_4 + H$	gas phase	(C3)
$CH_4 + H \rightarrow CH_3 + H_2$	gas phase	(C4)
$CH_3 + CH_3 \rightarrow C_2H_5 + H$	gas phase	(C5)
$C_2H_5 + H \rightarrow CH_3 + CH_3$	gas phase	(C6)
$CH_3 + CH_3 \rightarrow C_2H_6$	gas phase	(C7)
$C_2H_6 \rightarrow CH_3 + CH_3$	gas phase	(C8)
$C_2H_5 \rightarrow C_2H_4 + H$	gas phase	(C9)
$C_2H_4 + H \rightarrow C_2H_5$	gas phase	(C10)
$C_2H_4 \rightarrow C_2H_2 + H_2$	gas phase	(C11)
$C_2H_2 + H_2 \rightarrow C_2H_4$	gas phase	(C12)
$C_2H_5 \rightarrow 2C + 2.5H_2$	surface	(C13)
$C_2H_4 \rightarrow 2C + 2H_2$	surface	(C14)
$C_2H_2 \rightarrow 2C + H_2$	surface	(C15)
$CH_4 \rightarrow C + 2H_2$	surface	(C16)
$CH_3 \rightarrow C + 1.5H_2$	surface	(C17)

by basing this rate on the smaller of the surface mass fluxes, either silicon or carbon. This is analogous to enforcing a 1:1 stoichiometry at the growth surface, an approach that has been used in other silicon carbide CVD models [7,9].

3. ANALYSIS USING DIMENSIONLESS NUMBERS

A variety of dimensionless numbers exist which help to characterize CVD reactors, some of which are listed in Table 3. Analysis of reactors for organometallic vapor phase epitaxy (OMVPE) using dimensionless numbers has proved useful [12]. The values for the dimensionless numbers calculated for the silicon carbide reactor for two different pressures are given in Table 4. The characteristic length for the calculations was chosen as the distance between the susceptor and the top reactor wall.

At both pressures, the Knudsen number is much less than unity, indicating the applicability of continuum fluid dynamics to modeling the system. The Reynolds number indicates laminar flow, while the Prandtl number indicates that the relative magnitudes of the diffusion of momentum and heat through the gas phase are equivalent at both pressures. The Schmidt, thermal Peclet, and mass Peclet numbers indicate equal importance of transport by convection and by diffusion at

Table 3. Dimensionless numbers useful in CVD analysis.

Name	Description	Physical Interpretation
Knudsen	$Kn = \lambda/L$	$\frac{\text{mean free path}}{\text{characteristic length}}$
Reynolds	$Re = \frac{\langle v \rangle \cdot L}{\nu}$	$\frac{\text{momentum flux by convection}}{\text{momentum flux by diffusion}}$
Prandtl	$Pr = \frac{\upsilon}{\alpha}$	$\frac{\text{momentum diffusivity}}{\text{thermal diffusivity}}$
Schmidt	$Sc = \frac{\upsilon}{D}$	$\frac{\text{momentum diffusivity}}{\text{mass diffusivity}}$
Peclet (thermal)	$Pe_t = \frac{\langle v \rangle L}{\alpha}$	$\frac{\text{thermal flux by convection}}{\text{thermal flux by diffusion}}$
Peclet (mass)	$Pe_m = \frac{\langle v \rangle L}{D}$	$\frac{\text{mass flux by convection}}{\text{mass flux by diffusion}}$
Grashof (thermal)	$Gr_t = \frac{g\beta_t L^3 \Delta T}{\nu^2}$	$\frac{\text{momentum flux by free convection}}{\text{momentum flux by diffusion}}$
Rayleigh (thermal)	$Ra_t = \frac{g\beta_t L^3 \Delta T}{\nu\alpha}$	$\frac{\text{thermal flux by free convection}}{\text{thermal flux by diffusion}}$
Damkohler (convective)	$Da_c = \frac{k_g C^{n-1} L}{\langle v \rangle}$	$\frac{\text{characteristic time for flow}}{\text{characteristic time for gas phase reaction}}$
Damkohler (diffusive)	$Da_d = \frac{k_g C^{n-1} L^2}{D}$	$\frac{\text{characteristic time for diffusion}}{\text{characteristic time for gas phase reaction}}$
Damkohler (surface)	$Da_s = \frac{k_s L}{D}$	$\frac{\text{characteristic time for diffusion to surface}}{\text{characteristic time for surface reaction}}$

Table 4. Dimensionless numbers for the silicon carbide reactor.

Number	Species or Reaction	P = 2.7 kPa	P = 101 kPa
Knudsen	—	1×10^{-4}	3×10^{-6}
Reynolds	—	3	3
Prandtl	—	1	1
Grashof (thermal)	—	2×10^{-1}	$2 \times 10^{+2}$
Schmidt	SiH_4	2	2
	SiH_2	2	2
	Si_2H_6	2	2
	C_2H_4	2	2
	C_2H_2	2	2
	CH_4	2	2
	CH_3	2	2
Peclet (thermal)	—	3	3
Peclet (mass)	SiH_4	5	6
	SiH_2	5	5
	Si_2H_6	7	8
	C_2H_4	6	6
	C_2H_2	5	6
	CH_4	5	5
	CH_3	4	5
Rayleigh (thermal)	—	2×10^{-1}	$2 \times 10^{+2}$
Damkohler (convective)	$SiH_4 \rightarrow SiH_2 + H_2$	3×10^{-1}	1
	$SiH_2 + H_2 \rightarrow SiH_4$	$8 \times 10^{+1}$	$1 \times 10^{+5}$
	$C_3H_8 \rightarrow CH_3 + C_2H_5$	3×10^{-4}	4×10^{-4}
	$CH_3 + H_2 \rightarrow CH_4 + H$	$4 \times 10^{+1}$	$3 \times 10^{+4}$
	$CH_4 + H \rightarrow CH_3 + H_2$	2×10^{-2}	$8 \times 10^{+1}$
Damkohler (diffusive)	$SiH_4 \rightarrow SiH_2 + H_2$	1	8
	$SiH_2 + H_2 \rightarrow SiH_4$	$3 \times 10^{+2}$	$6 \times 10^{+5}$
	$C_3H_8 \rightarrow CH_3 + C_2H_5$	2×10^{-3}	2×10^{-3}
	$CH_3 + H_2 \rightarrow CH_4 + H$	$1 \times 10^{+2}$	1×10^{5}
	$CH_4 + H \rightarrow CH_3 + H_2$	8×10^{-2}	$4 \times 10^{+2}$
Damkohler (surface)	$SiH_4 \rightarrow Si + 2H_2$	7×10^{-2}	3
	$SiH_2 \rightarrow Si + H_2$	$3 \times 10^{+2}$	$1 \times 10^{+4}$
	$Si_2H_6 \rightarrow 2Si + 3H_2$	$3 \times 10^{+2}$	$1 \times 10^{+4}$
	$C_2H_4 \rightarrow 2C + 2H_2$	6×10^{-1}	$3 \times 10^{+1}$
	$C_2H_2 \rightarrow 2C + H_2$	6×10^{-1}	$3 \times 10^{+1}$
	$CH_4 \rightarrow C + 2H_2$	2×10^{-2}	7×10^{-1}
	$CH_3 \rightarrow C + 1.5H_2$	$3 \times 10^{+2}$	$1 \times 10^{+4}$

both pressures. The Grashof and Rayleigh numbers both drop by about three orders of magnitude as the pressure decreases from 101 kPa to 2.7 kPa, indicating the buoyancy driven flows become less important at lower pressures. Free convective effects should be significant at 101 kPa, as indicated by the large Grashof number.

Convective and diffusive Damkohler numbers were calculated for reactions in the chemistry set which were most likely to affect the silicon and carbon flux to the surface, and were found to decrease with pressure for all reactions listed. The exception was the gas-phase decomposition of propane, where the numbers remained relatively consistant with pressure at low values, indicating that the reaction is not proceeding to a large extent in the reaction zone. This implies that fewer carbon-containing species will be available for deposition than might otherwise be possible with a more reactive carbon source. The large surface Damkohler numbers at 101 kPa indicate that the species believed to be important in the deposition process are in the diffusion-controlled regime, except for SiH_4 and CH_4, which are in a mixed-control regime. Large concentration differences in a diffusion-controlled regime can lead to non-uniform deposits; this is in agreement with the observed non-uniform deposition of silicon carbide in a reactor operated at 101 kPa [13]. The surface Damkohler numbers decrease as the pressure decreases to 2.7 kPa, moving species toward a kinetically-controlled regime and the possibility of greater deposition uniformity.

The results presented here are still grid sensitive. Work is continuing to arrive at fully converged results. However, the important aspects of the chemistry and transport phenomena have been resolved, and the model predictions can provide useful qualitative results regarding the operation of the silicon carbide CVD reactor.

4. MODELING RESULTS

Streaklines were used to visualize the predicted flow. Streaklines are continuous lines that join all fluid particles originating from the same point in the fluid. For the steady-flow conditions in these simulations, streaklines are identical to streamlines. Figure 3 shows the path of particles introduced at a vertical position immediately above the susceptor surface at a pressure of 101 kPa. A large convective roll exits at the back of the reactor. The incoming gas rises as it is heated, is compressed into a narrow region, and flows in a relatively undisturbed manner over the center of the susceptor. Experimentally, this is the area which yields crystals with better surface morphology. Figure 4

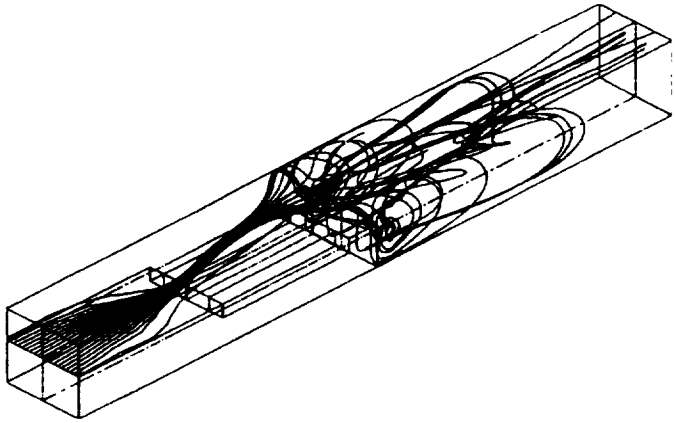

Figure 3. Streaklines in SIC CVD reactor. Particles introduced in a plane immediately above susceptor surface (P = 101 kPa).

shows the streaklines for particles introduced at a vertical distance midway between the susceptor and the top reactor wall. Tight convective rolls are observed along the sides of the susceptor, most likely the cause of the compressed flow seen in Figure 3. The convective roll in front of the susceptor can now be seen as well.

For a pressure of 2.7 kPa, Figure 5 shows streaklines for particles introduce in a plane immediately above the susceptor, while Figure 6

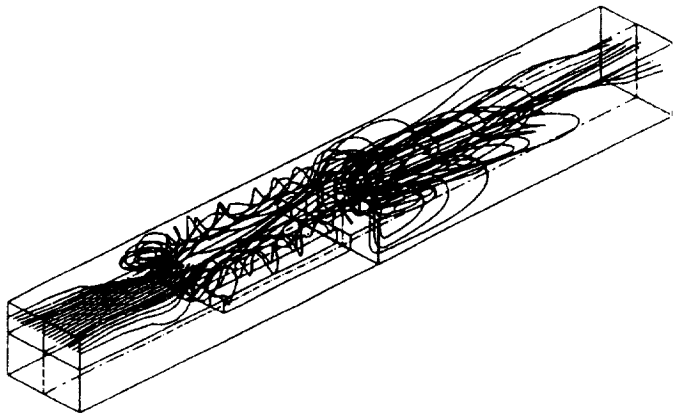

Figure 4. Streaklines in SiC CVD reactor. Particles introduced in a plane midway between susceptor surface and top reactor wall (P = 101 kPa).

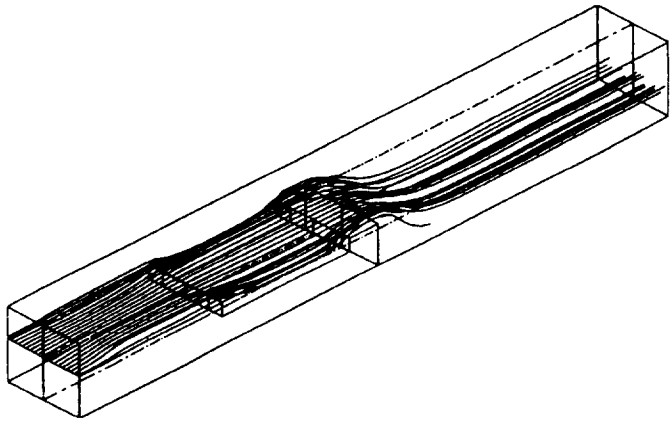

Figure 5. Streaklines in SIC CVD reactor. Particles introduced in a plane immediately above the susceptor (P = 2.7 kPa).

shows those for particles introduced midway between the susceptor surface and top reactor wall. The absence of recirculation is evident.

A comparison of the surface mole flux for both silicon and carbon at both 2.7 kPa and 101 kPa is shown along the susceptor centerline in Figure 7(a) and along the susceptor edge in Figure 7(b). The flatter curves at 2.7 kPa indicate a more axially uniform flux of silicon and carbon to the surface as compared to 101 kPa. Except near the leading

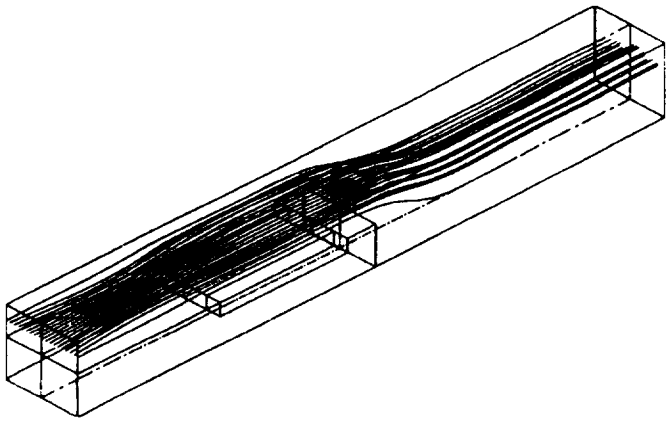

Figure 6. Streaklines in SiC CVD reactor. Particles introduced in a plane midway between susceptor surface and top reactor wall (P = 2.7 kPa).

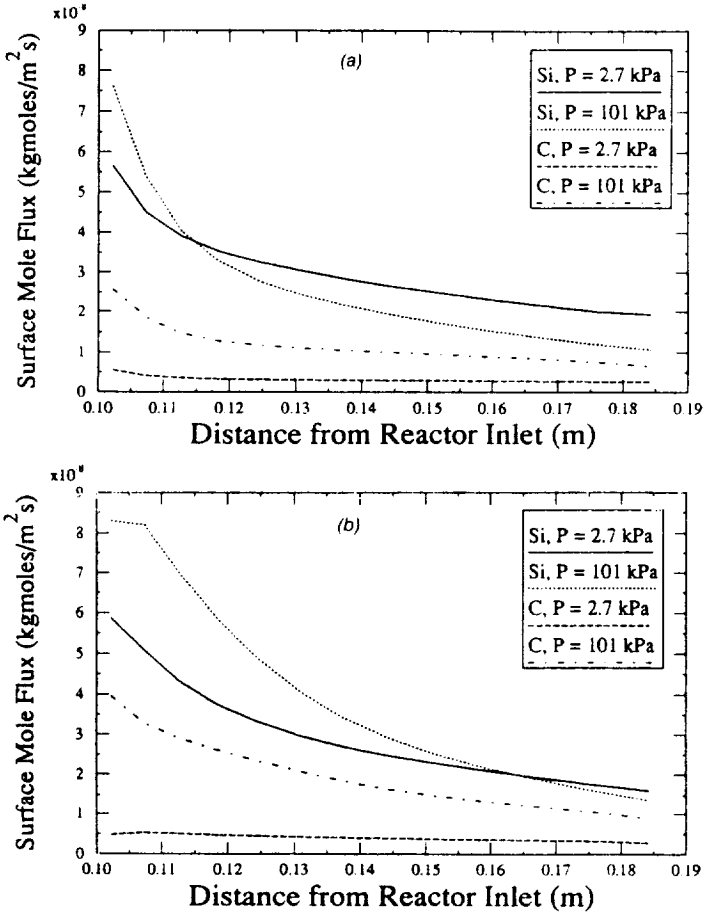

Figure 7. Surface mole flux of silicon and carbon at 2.7 kPa and 101 kPa: a) along susceptor centerline; b) alone the susceptor edge.

edge of the susceptor, the silicon mole flux to the surface is greater at 2.7 kPa than at 101 kPa, with the flux along the centerline rising about 43% midway along the susceptor length as the pressure decreases. The flux of carbon to the surface is always smaller at 2.7 kPa compared to 101 kPa, the decrease with pressure being about 70% along the centerline midway along the susceptor length. The flux of carbon to the surface limits the growth of silicon carbide at both pressures. The smooth flow of gases along the centerline at 101 kPa results in a greater depletion of species compared to the edges of the susceptor, and, therefore, a

lower flux of species to the surface. Convective rolls along the edges mix the depleted gases with more reactant-rich gases flowing along the reactor walls, providing additional gas phase reactants for deposition along the susceptor edges.

Figure 8 shows the contribution of individual species to the surface mass flux of silicon at 2.7 kPa and 101 kPa; Figure 9 is the corresponding figure for carbon species. SiH_2 is the major species contributing to the deposition of silicon at both 2.7 kPa and 101 kPa, although SiH_4 contributes a small, but noticeable amount at 101 kPa. C_2H_5 contrib-

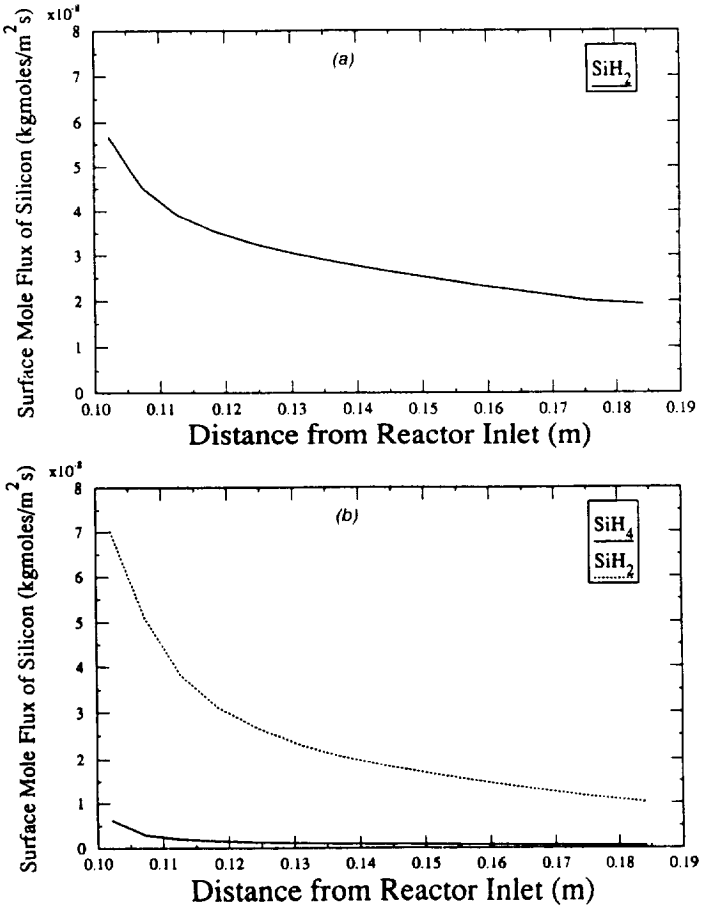

Figure 8. Contribution of major growth species to surface mole flux of silicon along susceptor centerline: a) 2.7 kPa; b) 101 kPa.

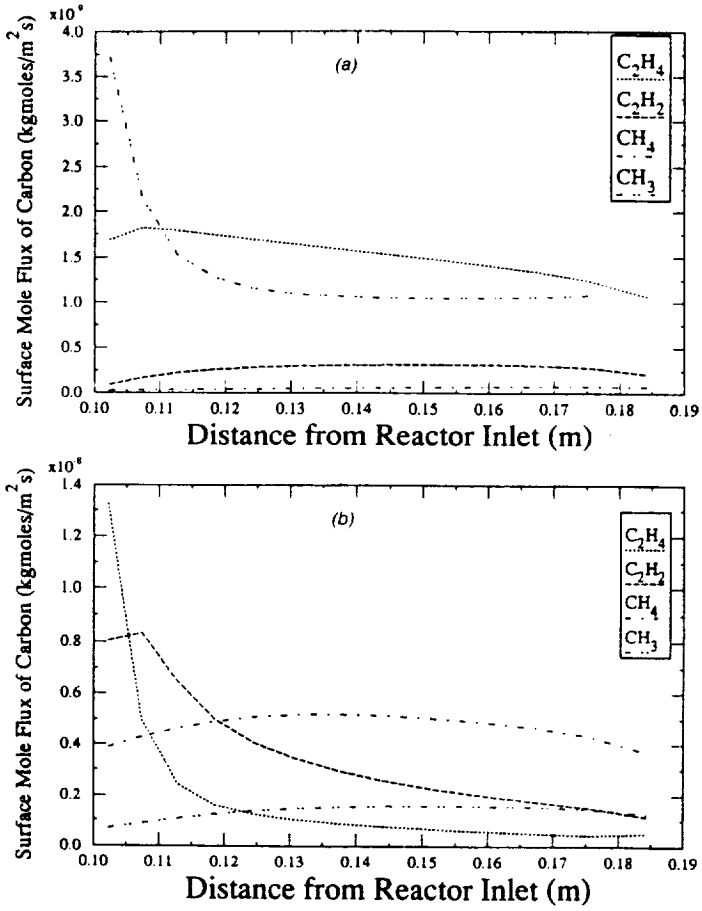

Figure 9. Contribution of major growth species to surface mole flux of carbon along susceptor centerline: a) 2.7 kPa; b) 101 kPa.

utes a negligible amount to carbon deposition, and is, therefore, not included in Figure 9. At 2.8 kPa, C_2H_4 contributes the most to the carbon flux along the centerline, with CH_3 contributing the next greatest amount. At 101 kPa, CH_4 is the dominant species contributing to carbon deposition; however, C_2H_4, C_2H_2, and CH_3 also contribute a significant amount to the carbon deposition.

Referring to Table 4, the convective and diffusive Damkohler numbers show that the characteristic time for convection or diffusion associated with SiH_4 dissociation is approximately the same at 2.7 kPa and

101 kPa, allowing for production of the highly reactive SiH_2 in the reaction zone above the deposition surface. The surface Damkohler number decreases significantly with pressure, indicating more rapid diffusion rates to the surface and, therefore, decreased depletion of gas phase species near the surface at lower pressures. This explains the higher net surface mole flux of silicon along the centerline at 2.7 kPa compared to 101 kPa. The convective and diffusive Damkohler numbers for propane at both pressures indicate that the characteristic time for reaction is much larger than that for flow or diffusion, implying that much of the propane will pass unreacted through the reaction zone. These Damkohler numbers are smaller for other reactions involving carbon-containing species at low pressures; therefore, fewer species which could contribute to carbon deposition will be present, and a lower molar flux of carbon to the surface will be observed at low pressures. At 101 kPa, the large surface Damkohler numbers indicate that most of the carbon-containing species are in or near the diffusion-controlled regime. These results agree with the nonuniform deposition observed experimentally at 101 kPa. At 2.7 kPa, where C_2H_4 and CH_3 are clearly dominant in carbon deposition, their surface Damkohler numbers indicate that there is mixed diffusion and kinetic control, indicating better deposition uniformity should result at 2.7 kPa compared to 101 kPa.

Since the flux of carbon to the growth surface was always less than that of silicon at 101 kPa along the susceptor centerline, the predicted silicon carbide deposition rate was based on the carbon flux to the surface. The predicted deposition rate of about 0.4 micron/hour was substantially less than the experimentally observed value of about four microns/hour. Further consideration of the experimental system revealed an additional source of silicon and carbon not accounted for in the model. The graphite susceptor is coated with polycrystalline silicon carbide which can be etched by the hydrogen carrier gas, thus supplying additional silicon and carbon into the system. While no experimental data could be found on the etch rate of polycrystalline silicon carbide, etch rates for single-crystal silicon carbide were found in the literature [14]. As a rough approximation, the etch rate of polycrystalline silicon carbide was assumed to be twice that of the single-crystal material; the amount of silicon and carbon entering the system due to etching was then found to be at least as much as that entering the system with the feed gas. This extra amount was included in the inlet concentration of reactant species in the model. Figure 10 compares the predicted surface mole flux of silicon and carbon with and without susceptor etching effects included at 101 kPa. The deposition rates for silicon and carbon increased by about 200% midway along the susceptor

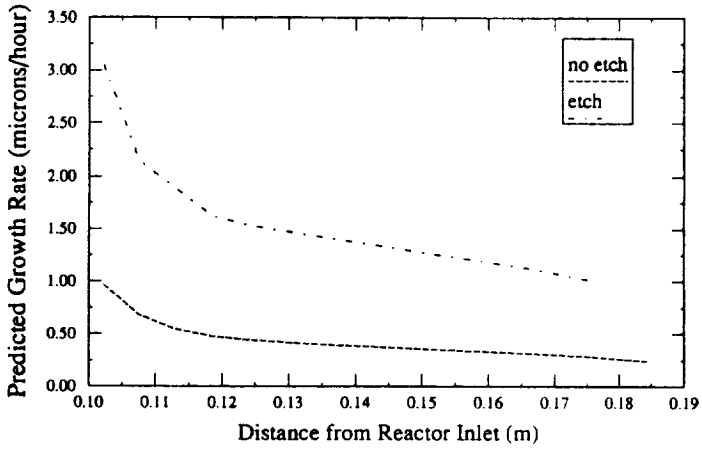

Figure 10. Predicted deposition rate of silicon carbide both with and without the effects of susceptor etchings included in the model.

length when the effects of susceptor etching are included, bringing the deposition rate up to bout 1.3 microns/hour, closer to the experimentally observed value.

5. CONCLUSIONS

The modeling results indicate that the growth rate of silicon carbide is limited by the availability of carbon, since at both 2.7 kPa and 101 kPa, the flux of silicon to the surface exceeds that of carbon. The low convective and diffusive Damkohler numbers for propane decomposition indicate that this reaction is not occurring to a large extent in the gas phase before propane leaves the reaction zone. An increase in the operating temperature would increase the propane decomposition, but would also result in an increase in the convective rolls observed in the system, with a corresponding decrease in the deposition uniformity. A more reactive carbon source would decompose more quickly to reactive intermediate species which could increase the carbon deposition rate, and hence, the silicon carbide growth rate. This growth rate is also limited to a lesser extent by the depletion of reactant species in the gas phase, particularly at 101 kPa. While this depletion becomes less severe for silicon and carbon at 2.7 kPa compared to 101 kPa, the flux of species to the surface also decreases with pressure, resulting in an overall lower deposition rate.

The more nonuniform deposition at 101 kPa compared to 2.7 kPa results mainly from the convective rolls present in the reactor and the diffusion-controlled regime existing for the major deposition species at 101 kPa. Deposition uniformity is closely tied to gas flow patterns in a diffusion-controlled regime, and while the flow is relatively undisturbed through the center of the growth surface, convective rolls protude along the edges, as well as the front, of the susceptor. These differing gas flow patterns will result in differing compositions of gas-phase species above the growth surface, and hence, differing deposition rates. The convective rolls mix reactant-rich gases away from the susceptor with depleted gas along the susceptor edge, raising the reactant concentration, and hence the deposition rate along the susceptor edge. The convective rolls do not reach the center of the susceptor; therefore, depleted gases are not replenished with additional reactants. As the pressure is reduced to 2.7 kPa, the major depositing species move away from a diffusion-controlled regime into a mixed-control, or even a kinetic-controlled, regime, where the deposition is not dependent on the gas-flow patterns and species concentrations tend to be more uniform over the growth surface. Even for those species still in the diffusion-controlled regime at 2.7 kPa, a uniform flow pattern exists over the growth surface, leading to improved deposition uniformity. A decrease in depletion of reactive species also results as the pressure is lowered, resulting in better deposition uniformity along the length of the growth surface.

The model indicates that the amount of silicon and carbon entering the system is not well characterized. The quality of species entering the system through etching of the silicon-carbide coated susceptor is unknown. Model predictions of silicon carbide growth rate without including the effects of susceptor etching are much too low. A rough approximation as to the effects of susceptor etching results in a predicted deposition rate that, while still low, is much closer to the experimental value. Further experimental and modeling work is necessary, to better characterize this uncontrolled source of silicon and carbon entering the growth system.

NOTATION

Symbol	Description	Units
A	Arrhenius preexponential factor	$\text{time}^{-1}/\text{concentration}^{n-1}$
C	concentration	kgmoles/m^3

NOTATION (continued)

Symbol	Description	Units
D	diffusion coefficient	m^2/s
D_i^T	thermal diffusion coefficient	kg/m^2
D_i	diffusion coefficient of species i	kg/m^2
E_a	activation energy	J/kgmole
g	gravitational constant	m/s^2
h	enthalpy	J/kg
J_i	flux of species i	dimensionless
k	thermal conductivity	W/m K
k_g	gas-phase reaction rate constant	$time^{-1}/concentration^{n-1}$
k_s	surface reaction rate constant	$time^{-1}/concentration^{n-1}$
k_w	thermal conductivity of wall	W/m K
L	characteristic length	m
M_i	molecular weight	kg/kgmoles
n	reaction order	dimensionless
$\hat{n}$	unit vector normal to surface	m
P	pressure	Pa
R	universal gas constant	J/kgmoles K
R_i	mass rate of creation or depletion of species i by chemical reaction	kg/m^3 s
S_i	sticking coefficient of species i	dimensionless
T	temperature	K
ΔT	characteristic temperature difference	K
u_i	velocity in the ith direction	m/s
(v)	average velocity	m/s
V_{ik}	molar stoichiometry coefficient for species i in reaction k	dimensionless
x_i	distance in the ith direction	m
X_i	mass fraction of species i	dimensionless
α	thermal diffusivity	m^2/s
β	temperature exponent for Arrhenius rate expression	dimensionless
β_T	coefficient of volume expansion	K^{-1}
λ	mean free path	m
ϱ	density	kg/m^3
μ	Newtonian viscosity	kg/m s
ν	kinematic viscosity	m^2/s
ν_{jk}	exponent on concentration of reactant j in reaction k	dimensionless

APPENDIX A: REACTION RATE CONSTANTS FOR SILICON CHEMISTRY

Reaction	A*	β	E_a (J/kgmoles K)	
$SiH_4 \rightarrow SiH_2 + H_2$	6.1E + 28	−5	2.461E + 8	(S1)
$SiH_2 + H_2 \rightarrow SiH_4$	5.28E + 21	−4.4	1.427E + 7	(S2)
$Si_2H_6 \rightarrow SiH_4 + SiH_2$	2.12E + 35	−6.47	2.360E + 8	(S3)
$SiH_4 + SiH_2 \rightarrow Si_2H_6$	1.79E + 24	−4.5	1.284E + 7	(S4)
$SiH_4 \rightarrow Si + 2H_2$	3.453E − 1	0.5	7.816E + 7	(S5)
$SiH_2 \rightarrow Si + H_2$	6.641	0.5	0	(S6)
$Si_2H_6 \rightarrow 2Si + 3H_2$	4.62	0.5	0	(S7)

*Units are kgmoles, m³, s.

Reactions S1–S4 occur in the gas phase; reactions S5–S7 are surface reactions.

APPENDIX B: REACTION RATE CONSTANTS FOR CARBON CHEMISTRY

Reaction	A*	β	E_a (J/kgmoles K)	
$C_3H_8 \rightarrow CH_3 + C_2H_5$	5E + 15	0	3.5E + 8	(C1)
$CH_3 + C_2H_5 \rightarrow C_3H_8$	7E + 9	0	0	(C2)
$CH_3 + H_2 \rightarrow CH_4 + H$	6.6E − 1	3	3.24E + 7	(C3)
$CH_4 + H \rightarrow CH_3 + H_2$	2.2E + 1	3	3.66E + 7	(C4)
$CH_3 + CH_3 \rightarrow C_2H_5 + H$	8E + 11	0	1.11E + 8	(C5)
$C_2H_5 + H \rightarrow CH_3 + CH_3$	3E + 10	0	0	(C6)
$CH_3 + CH_3 \rightarrow C_2H_6$	2.4E + 11	−0.4	0	(C7)
$C_2H_6 \rightarrow CH_3 + CH_3$	2.4E + 16	0	3.66E + 8	(C8)
$C_2H_5 \rightarrow C_2H_4 + H$	4.89E + 9	1.19	1.56E + 8	(C9)
$C_2H_4 + H \rightarrow C_2H_5$	8.42E + 5	1.49	4.15E + 6	(C10)
$C_2H_4 \rightarrow C_2H_2 + H_2$	7.95E + 12	0.44	3.71E + 8	(C11)
$C_2H_2 + H_2 \rightarrow C_2H_4$	3.01E + 8	0	1.63E + 8	(C12)
$C_2H_5 \rightarrow 2C + 2.5H_2$	6.748	0.5	0	(C13)
$C_2H_4 \rightarrow 2C + 2H_2$	1.37E − 2	0.5	0	(C14)
$C_2H_2 \rightarrow 2C + H_2$	1.43E − 2	0.5	0	(C15)
$CH_4 \rightarrow C + 2H_2$	4.5E − 4	0.5	0	(C16)
$CH_3 \rightarrow C + 1.5H_2$	9.381	0.5	0	(C17)

*Units are kgmoles, m³, s.

Reactions C1–C12 occur in the gas phase; reactions C13–C17 are surface reactions.

REFERENCES

1. FLUENT is a computer program for modeling fluid flow, heat transfer, and chemical reaction, from Fluent, Inc., Lebanon, NH, 03766.
2. Sheikholeslami, M. Z., T. Jasinski and K. W. Fretz. 1988. "Numerical Modeling of Chemical Vapor Deposition (CVD) in a Horizontal Reactor," *Proceedings AIAA First National Fluid Dynamic Congress,* Cincinnati, OH, pp. 1616–1620.
3. Gokoglu, S. A., M. Kuczmarski, L. Veitch, P. Tsui and A. Chait. 1990. "A Numerical and Experimental Analysis of Reactor Performance and Deposition Rates for CVD on Monofilaments," *Proceedings Eleventh International Conference on Chemical Vapor Deposition–1990, Proceedings 90-12,* K. E. Spear, G. W. Cullen, eds., The Electrochemical Society, pp. 31–37.
4. Gokoglu, S. A., M. Kuczmarski and L. C. Veitch. 1992. "Prediction of Chemical Vapor Deposition Rates on Monofilaments and Its Implications for Fiber Properties," *J. Mater. Res.,* 7(11):3023–3031.
5. Fischman, G. S. and W. T. Petusky. 1985. "Thermodynamic Analysis and Kinetic Implications of Chemical Vapor Deposition of SiC from Si-C-Cl-H Gas Systems," *J. Am. Ceramic Soc.,* 68(4):185–190.
6. Stinespring, C. D. and J. C. Wormhoudt. 1988. "Gas Phase Kinetic Analysis and Implications for Silicon Carbide Chemical Vapor Deposition," *J. Crystal Growth,* 87:481–493.
7. Stinespring, C. D., K. D. Annen and J. C. Wormhoudt. 1988. "Optimization of Silicon Carbide Production," *ARI-RR-656* (Aerodyne Research Inc., Billerica, MA.)
8. Moffat, H. K. and K. F. Jensen. 1988. "Three-Dimensional Flow Effects in Silicon CVD in Horizontal Reactors," *J. Electrochem. Soc.,* 135(2):459–471.
9. Allendorf, M. D. and R. J. Kee. 1991. "A Model of Silicon Carbide Chemical Vapor Deposition," *J. Electrochem. Soc.,* 138(3):841–852.
10. 1990. NIST Chemical Kinetics Database, Version 2.0, U.S. Department of Commerce, National Institute of Standards and Technology, Standard Reference Data Program, Gaithersburg, MD.
11. Annen, K. D., C. D. Stinespring, M. A. Kuczmarski and J. A. Powell. 1990. "Modeling of the SiC Chemical Vapor Deposition Process and Comparison with Experimental Results," *J. Vac. Sci. Technol. A,* 8(3):2970–2975.
12. Jensen, K. F. 1989. "Transport Phenomena and Chemical Reaction Issues in OMVPE of Compound Semiconductors," *J. Cryst. Growth,* 98:148–166.
13. Powell, J. A., L. G. Matus and M. A. Kuczmarski. 1987. "Growth and Characterization of Cubic SiC Single Crystal Films on Si," *J. Electrochem. Soc.,* 134(6):1558–1565.
14. Saidov, M. S., Kh. A. Shamuratov and M. A. Kadyrov. 1988. "Study of Growth Conditions of Silicon Carbide Epitaxial Layers," *J. Cryst. Growth,* 87:519–522.